Interrelationships between structure and function during the hemostatic response to injury

Maurizio Tomaiuolo[a], Chelsea N. Matzko[a], Izmarie Poventud-Fuentes[a], John W. Weisel[b], Lawrence F. Brass[a], and Timothy J. Stalker[a,1]

[a]Department of Medicine, Perelman School of Medicine, University of Pennsylvania, Philadelphia, PA 19104; and [b]Department of Cell and Developmental Biology, Perelman School of Medicine, University of Pennsylvania, Philadelphia, PA 19104

Edited by Barry S. Coller, The Rockefeller University, New York, NY, and approved December 20, 2018 (received for review August 15, 2018)

Extensive studies have detailed the molecular regulation of individual components of the hemostatic system, including platelets, coagulation factors, and regulatory proteins. Questions remain, however, about how these elements are integrated at the systems level within a rapidly changing physical environment. To answer some of these questions, we developed a puncture injury model in mouse jugular veins that combines high-resolution, multimodal imaging with functional readouts in vivo. The results reveal striking spatial regulation of platelet activation and fibrin formation that could not be inferred from studies performed ex vivo. As in the microcirculation, where previous studies have been performed, gradients of platelet activation are readily apparent, as is an asymmetrical distribution of fibrin deposition and thrombin activity. Both are oriented from the outer to the inner surface of the damaged vessel wall, with a greater extent of platelet activation and fibrin accumulation on the outside than the inside. Further, we show that the importance of $P2Y_{12}$ signaling in establishing a competent hemostatic plug is related to the size of the injury, thus limiting its contribution to hemostasis to specific physiologic contexts. Taken together, these studies offer insights into the organization of hemostatic plugs, provide a detailed understanding of the adverse bleeding associated with a widely prescribed class of antiplatelet agents, and highlight differences between hemostasis and thrombosis that may suggest alternative therapeutic approaches.

hemostasis | platelets | coagulation | thrombin | P2Y12

The hemostatic response in humans and other mammals is a complex process that requires both cellular and molecular components of the blood. Its goal is to halt the loss of blood after a breach in a closed, high-pressure circuit. When it fails, as it can in settings as disparate as trauma and coagulation factor deficiencies, life-threatening bleeding can result. Considerable effort during the last several decades has been made to understand this process, focusing on individual coagulation reactions and the identification of receptors and signaling pathways within platelets. Those studies have most commonly employed a reductionist approach, attempting to understand the behavior of a complex system through the study of its isolated parts, often under static rather than dynamic conditions, and more frequently studied ex vivo than in vivo.

Recently, we and others have returned to an earlier, systems-oriented perspective, investigating how the multitude of now well-defined molecular mechanisms regulating coagulation and platelet activation are integrated within the dynamic physical environment present at sites of vascular injury in vivo. A model of the hemostatic response has emerged from those studies in which it is now clear that gradients of platelet agonists such as thrombin, ADP, and TxA_2 are shaped by physical forces present within the evolving platelet plug, resulting in a gradient of platelet activation emanating from the injury site (1). Those physical forces arise in part from the consequences of piling up platelets, and in part from the contraction of activated platelets. The net result is a hierarchical architecture in which the spatial distribution of activated platelets and fibrin is tightly regulated, an architecture that is very different from the structure of pathological thrombi in either the arterial or venous circulations (2–4). In the studies published to date, the ability to reconstruct these events rests in part on real-time imaging performed in vivo in transgenic mouse models, and in part on computational studies (5–8).

For technical reasons, the initial evidence describing the hierarchical organization of hemostatic plugs was derived primarily from observations in the mouse microvasculature after small (<5 μm) penetrating injuries, leaving unanswered whether the conclusions are specific to the microcirculation or are more generalizable. These studies were recently extended to the femoral artery and saphenous vein, although again the injuries were small (10–15 μm) and resulted in minimal bleeding (9). Questions therefore remain regarding the relationship between hemostatic plug organization and bleeding when the blood vessel and injury size are sufficient to cause substantial blood loss. In these contexts, a large pressure drop occurs across the injury site and the resulting convective forces as blood escapes are expected to substantially affect the spatiotemporal regulation of platelet and coagulation system activation, likely in ways that are different from pathologic settings that lead to thrombosis without bleeding.

The studies presented here are intended to answer these questions by combining high-resolution, multimodal imaging with functional readouts in vivo to examine the hemostatic response in

Significance

Extensive studies have detailed the molecular regulation of individual components of the hemostatic system. Important questions remain, however, regarding how elements of the coagulation cascade, platelets, and the vessel wall are integrated at the systems level to achieve hemostasis in vivo. Here, in a series of high-resolution imaging studies, we explore in detail how a hemostatic plug composed of platelets and fibrin forms in the setting of penetrating vascular injuries. The results reveal a surprisingly heterogeneous hemostatic plug architecture, including gradients of platelet activation and spatial sequestration of thrombin activity outside the vessel lumen. They also show how a widely prescribed class of antiplatelet agents alters hemostatic plug architecture, resulting in adverse bleeding in certain physiologic contexts.

Author contributions: M.T. and T.J.S. designed research; M.T., C.N.M., I.P.-F., and T.J.S. performed research; M.T., C.N.M., I.P.-F., J.W.W., L.F.B., and T.J.S. analyzed data; and M.T. and T.J.S. wrote the paper.

The authors declare no conflict of interest.

This article is a PNAS Direct Submission.

[1]To whom correspondence should be addressed. Email: tstalker@pennmedicine.upenn.edu.

This article contains supporting information online at www.pnas.org/lookup/suppl/doi:10.1073/pnas.1813642116/-/DCSupplemental.

Published online January 23, 2019.

a way that has not been done before. The results show that some of the conclusions drawn from studies in the microvasculature are in fact scalable to the macrovasculature, despite large differences in blood flow, vessel wall composition, vessel wall thickness, and injury size. The results also speak to the contribution of ADP in the setting of larger injuries, the spatially restricted contribution of platelet procoagulant activity, the adverse effect of a widely prescribed class of antiplatelet agents, and the apparent lack of a requirement for dense red cell packing to the achievement of an effective hemostatic response. The results also show that adopting a structure-and-function approach at the cellular as well as the molecular level offers insights into the organization of hemostatic plugs and highlights critical differences between hemostasis and thrombosis.

Results

A Model for Examining the Composition and Morphology of Hemostatic Plugs in Large Veins. We developed a mouse jugular vein puncture injury model to examine hemostatic plug formation in the macrocirculation. The jugular vein of a mouse was exposed and pierced with a 30-gauge needle (300 μm diameter), followed by fixation at predetermined points. The time until bleeding stopped was recorded as the bleeding time. A multimodal, correlative microscopy approach was used to examine the resulting hemostatic response. Confocal and 2-photon fluorescence imaging provided detail of molecular components, such as the localization of the platelet activation marker P-selectin and formation of fibrin, followed by scanning electron microscopy (SEM) of the same hemostatic plugs to observe cellular composition and detailed morphological features at high resolution. Different hemostatic plugs were prepared and observed from either the intravascular or extravascular side of the blood vessel to compare molecular and structural features in these two regions.

Platelet Activation Gradients and Hierarchical Organization of Hemostatic Plugs. In response to puncture injury of the jugular vein, a large hemostatic plug formed over the injury site on the intraluminal side of the vessel wall (Fig. 1 *A*–*C*). In addition to the images included in Fig. 1, Movie S1 shows a 3D reconstruction of the same hemostatic plug based on fluorescence imaging, and an interactive image file shows additional SEM views (Dataset S1; video and dataset legends are included in the *SI Appendix*). Jugular vein hemostatic plugs were composed almost exclusively of platelets, with minimal incorporation of red blood cells. Virtually no white blood cells were observed during the hemostatic phase of the response to injury (up to 5 min postinjury), consistent with prior studies performed in the microcirculation (10).

Multiple platelet morphologies were observed demonstrating a gradient of platelet activation extending from the injury site.

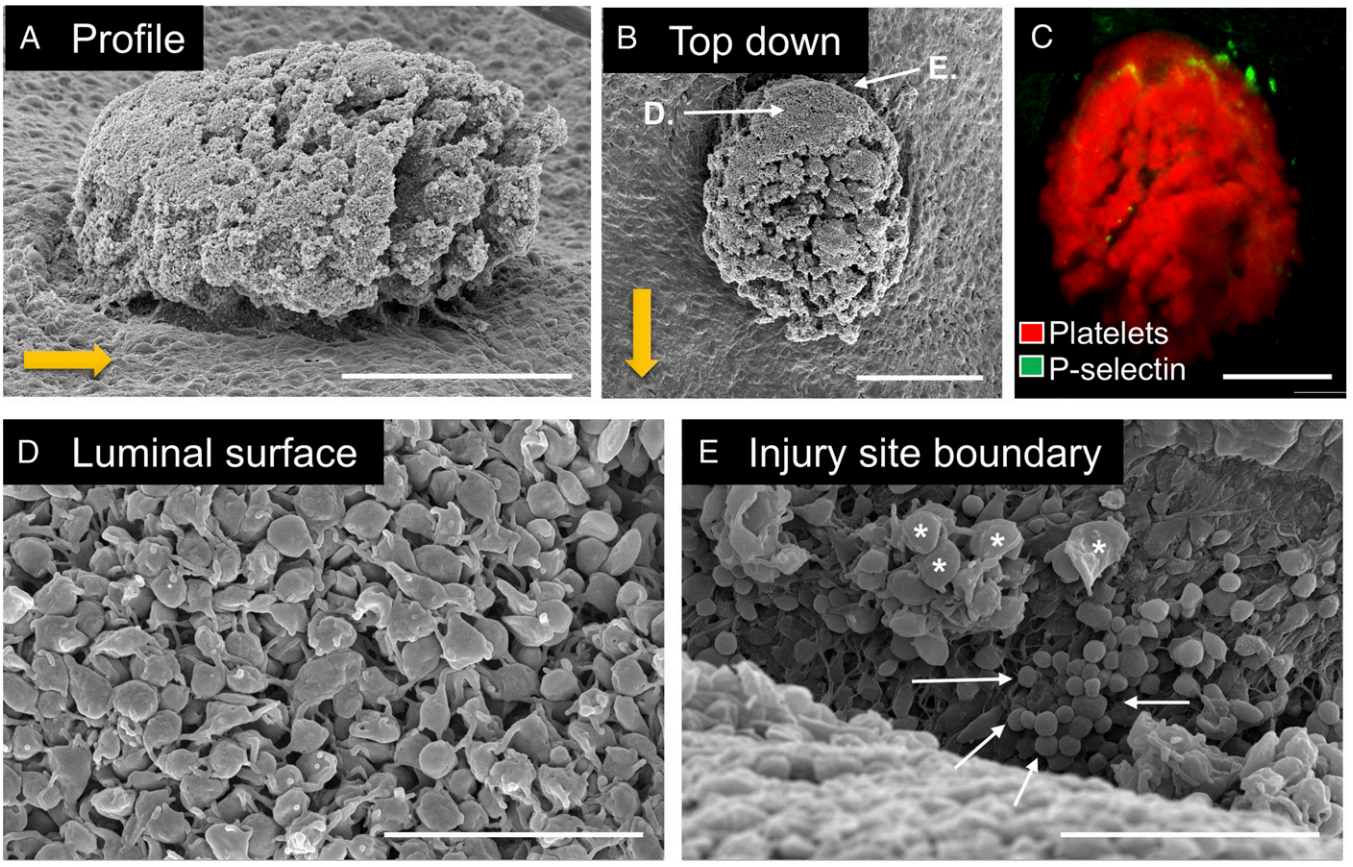

Fig. 1. Jugular vein hemostatic plug morphology: intravascular side. (*A*) Low-magnification SEM image of a representative hemostatic plug fixed 5 min postinjury. (Scale bar: 100 μm.) The sample is tilted to provide a profile view. Gold arrow indicates direction of blood flow. (*B*) The same hemostatic plug shown in *A* viewed from above. (Scale bar: 100 μm.) Locations of the zoomed images shown in *D* and *E* are indicated. Gold arrow indicates direction of blood flow. (*C*) Corresponding fluorescence image of the same hemostatic plug shown in *A* and *B*, oriented as in *B*. (Scale bar: 100 μm.) The image is a maximum intensity projection of a series of z-plane images acquired using 2-photon microscopy. A 3D reconstruction of the fluorescence images is included in Movie S1. (*D* and *E*) Higher magnification (Scale bar: 10 μm.) images of the regions indicated in *B*. White arrows (*E*) indicate platelets that appear to have fragmented into smaller vesicular bodies. Asterisks note intact platelets in the same field of view. Micrographs shown are representative of >10 hemostatic plugs imaged from the intravascular side 5 min postinjury. An interactive image file presenting multiple perspectives of the hemostatic plug shown is included in the *SI Appendix* (Dataset S1).

On the luminal surface, platelets exhibited morphologic features indicating minimal activation (Fig. 1*D*). Many of these platelets retained a discoid shape or had changed shape minimally, protruding a small number of projections. In some cases, spindle-shaped platelets were observed, elongated in the direction of flow. Consistent with a minimal activation state, platelets on the luminal surface of hemostatic plugs were also P-selectin-negative, indicating that they had not undergone α-granule exocytosis (Fig. 1*C*). Importantly, despite their apparent minimal activation state, platelets on the luminal surface were closely associated with one another and resisted dislodgment during wash procedures, indicating cohesive interactions (Fig. 1*D*).

In sharp contrast, platelets at the boundary of the injury site and within the hole created by the injury had a dramatically altered morphology. Platelets in this region were characterized by ultradense packing, such that cell bodies were squeezed tightly together, interwoven with filopods (Fig. 1*E* and Dataset S1). A striking feature in this region was the presence of numerous platelets that appeared to be fragmented, resulting in small spheroidal bodies ~0.5–1 μm in diameter (Fig. 1*E*, white arrows). In some cases, these bodies appeared to be the result of platelets squeezed so tightly together that a portion of the cell protrudes out into open space, whereas in other cases, these bodies may be distinct structures (microvesicles). In all cases, these dramatically altered cell morphologies were derived from platelets, as they were CD41 positive. When viewed from the lumen, P-selectin positivity (indicating robust platelet activation including α-granule secretion) was also observed primarily at the injury site boundary (Fig. 1*C* and Movie S1). Fibrin was sometimes observed here as well, but was otherwise largely absent from the platelet mass that formed on the intraluminal side of the injury site, as observed using either SEM or fluorescence imaging. In intermediate layers of hemostatic plugs, platelets appeared activated, but remained intact, with a more rounded appearance and abundant filopods (Dataset S1). Again, they were densely packed and no other cell types were observed.

Platelet and Fibrin Deposition Viewed from the Extravascular Perspective. The extravascular portion of the hemostatic plug had a dramatically different appearance than the intravascular portion (Fig. 2). Rather than a condensed platelet mass localized over the injury site, the extravascular portion of the hemostatic plug was characterized by platelets colocalized with an extensive fibrin network over a large surface area extending well beyond the edge of the injury site (Fig. 2 *A*–*C*, Dataset S2, and Movie S2). The majority of platelets found on the extravascular side of the vessel were highly activated and similar in morphology to the highly activated platelets observed at the boundary of the injury site when viewed from the intravascular side (Fig. 2 *D* and *E*). Platelet adhesion at the periphery of the injury site on the extravascular side resulted in significantly increased total platelet volume in this region compared with the intraluminal portion of

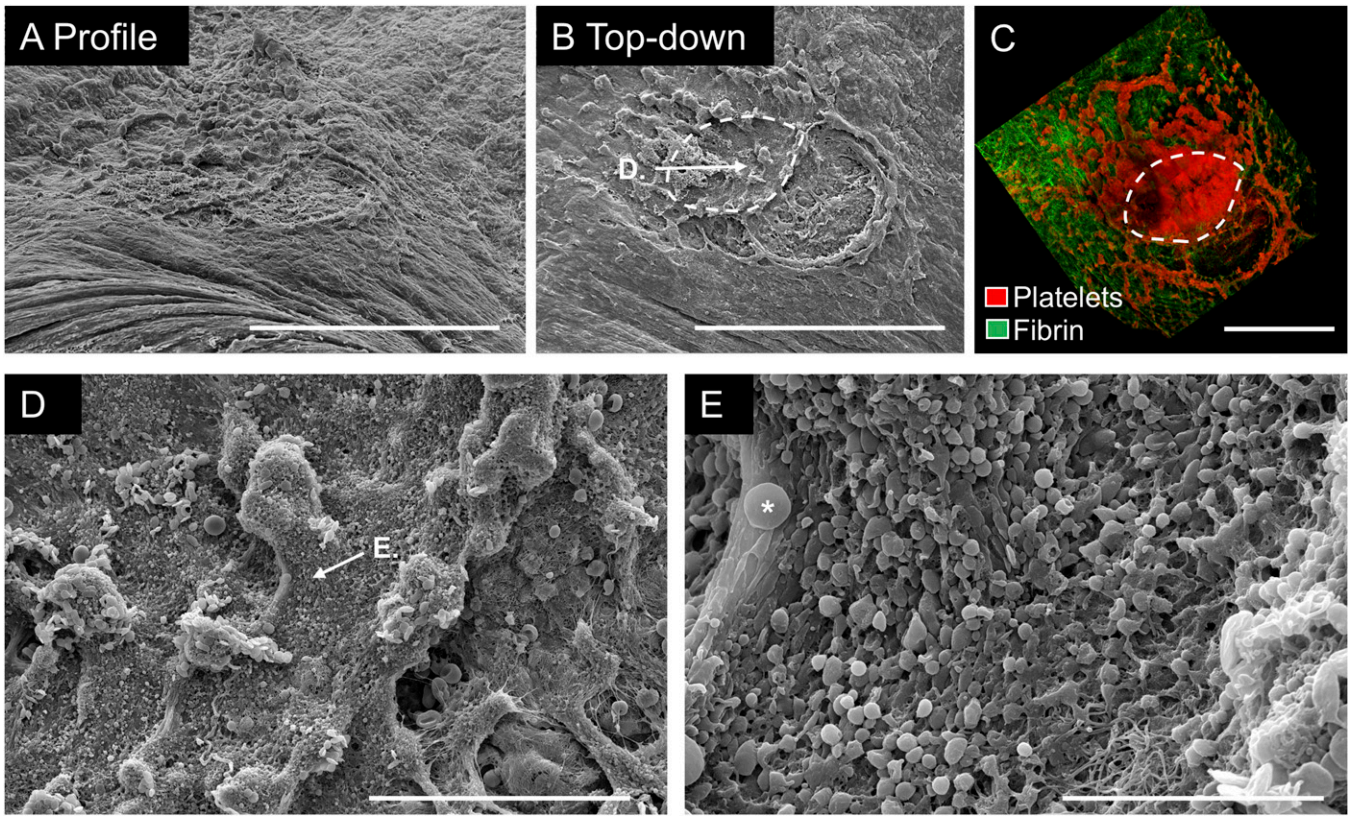

Fig. 2. Jugular vein hemostatic plug morphology: extravascular side. (*A*) Low-magnification SEM image of a representative hemostatic plug fixed 5 min postinjury. (Scale bar: 300 μm.) The sample is tilted to provide a profile view. (*B*) The same hemostatic plug shown in *A* viewed from above. (Scale bar: 300 μm.) Location of the zoomed image shown in *D* is indicated. (*C*) Corresponding fluorescence image of the same hemostatic plug shown in *A* and *B*, oriented as in *B*. The image is a maximum-intensity projection of a series of z-plane images acquired using 2-photon microscopy. A 3D reconstruction of the fluorescence images is included in Movie S2. Dotted line in *B* and *C* indicates the injury site. (Scale bar: 300 μm.) (*D*) Higher-magnification image of the region indicated in *B*, showing abundant highly activated platelets interspersed with fibrin at the injury site. (Scale bar: 50 μm.) (*E*) Higher-magnification image of the region indicated in *D* showing highly activated platelets. (Scale bar: 10 μm.) Some fibrin is also seen at the lower right of the image. Asterisk notes an intact platelet in the same field of view for comparison. Micrographs shown are representative of >10 hemostatic plugs imaged from the extravascular side 5 min postinjury. An interactive image file presenting multiple perspectives of the hemostatic plug shown is included in the *SI Appendix* (Dataset S2).

the hemostatic plug (Fig. 3 *A*–*C*). Platelet P-selectin was also highly expressed on the extravascular side of the injury site, indicating robust platelet activation with α-granule secretion, compared with the minimal P-selectin expression observed intraluminally (Fig. 3 *A*, *B*, and *E*; $P < 0.01$). Platelets uniformly filled the hole created by the injury (Figs. 2 *A*–*C* and 3*B*). They also formed smaller islands interconnected by fibrin fibers as they adhered to the extravascular surface of the blood vessel at the periphery of the injury site (Fig. 2*B*). Red blood cells were often observed trapped in the fibrin network (Fig. 2*D* and Dataset S2), but were a minimal component relative to platelets and fibrin.

The different platelet activation states observed between the extravascular and intravascular portions of hemostatic plugs using SEM and fluorescence imaging demonstrate the existence of a gradient of platelet activation, with the most robustly activated platelets at the base of the plug on the extravascular side, and the least activated platelets on the luminal surface on the intravascular side. This gradient of platelet activation overlapped with a striking asymmetric distribution of fibrin deposition, which was restricted almost entirely to the portion of the hemostatic plug filling the hole in the vessel wall and extending into the extravascular space (Fig. 4). These regional distributions of platelet activation and fibrin localization are also clearly visible in cryosections of separate samples. Cross-sections of hemostatic plugs showed P-selectin-positive platelets at the base of plugs extending into the extravascular space, whereas the platelets extending into the lumen on the intravascular side were P-selectin-negative (*SI Appendix*, Fig. S1 *A*–*C*). Fibrin deposition was similarly localized primarily outside of the vessel lumen (*SI Appendix*, Fig. S1*D*).

Time Course of Hemostatic Plug Formation. The hemostatic response was observed in the same manner 1, 5, and 20 min after injury. Although a fully mature hemostatic plug had not yet been formed 1 min postinjury, several of the morphological features described at 5 min postinjury (Figs. 1 and 2) were already present (*SI Appendix*, Fig. S2). Highly activated platelets were observed at the boundary of the injury site and on the extravascular portion of the hemostatic plug 1 min postinjury, demonstrating that these platelets are robustly activated rapidly on injury (*SI Appendix*, Fig. S2*A*). Fibrin was also already abundant on the extravascular side of the vessel. On the intravascular side, the developing platelet mass was incomplete, with platelets accumulated to the largest extent around the edge of the hole (*SI Appendix*, Fig. S2*B*). This is consistent with real-time imaging findings from prior studies showing that platelet aggregation initiates at the edge of the injury site, and the center of the hole is filled in as platelets continue to accumulate (11). By 5 min postinjury, a large platelet mass had formed over the hole, although it typically had a "cauliflower"-type appearance, with crevasses separating large columns of platelet aggregates (Fig. 1). 3D reconstructions of hemostatic plugs after optical sectioning using 2-photon microscopy demonstrated the existence of large open spaces within the volume of the platelet aggregate that were often connected to the aggregate surface (Movie S1). These open spaces are consistent with the appearance of platelet

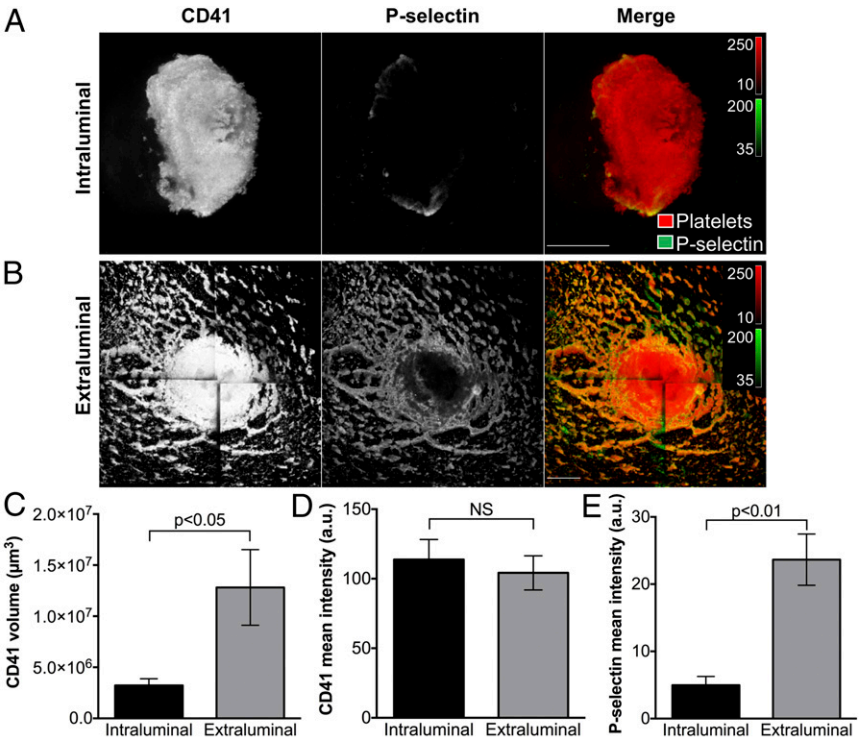

Fig. 3. Platelet alpha-granule secretion in the intraluminal and extravascular portions of mouse jugular vein hemostatic plugs. (*A* and *B*) Micrographs show a representative hemostatic plug fixed 5 min after puncture injury. The *Top* panels (*A*) show the intraluminal portion and *Bottom* panels (*B*) show the extraluminal portion of the same hemostatic plug imaged from each side. The images are maximum-intensity projections of a series of z-plane images acquired using 2-photon microscopy. Platelets (CD41, *Left* panels and red in the merge) and P-selectin expression (*Middle* panels, green in the merge) are shown. (Scale bars: 100 μm.) (*C*) The platelet volume in the intraluminal and extraluminal portions was calculated from the CD41 fluorescence. (*D*) CD41 fluorescence intensity (mean fluorescence intensity per pixel) in the intraluminal and extraluminal portions of hemostatic plugs. (*E*) P-selectin fluorescence intensity (mean fluorescence intensity per pixel) in the intraluminal and extraluminal portions of hemostatic plugs. CD41 and P-selectin quantification was performed on $n = 5$ hemostatic plugs as described in the *SI Appendix*, *Supplemental Methods*. Graphs show mean ± SEM; statistics were performed using a Student's *t* test. NS indicates not significant.

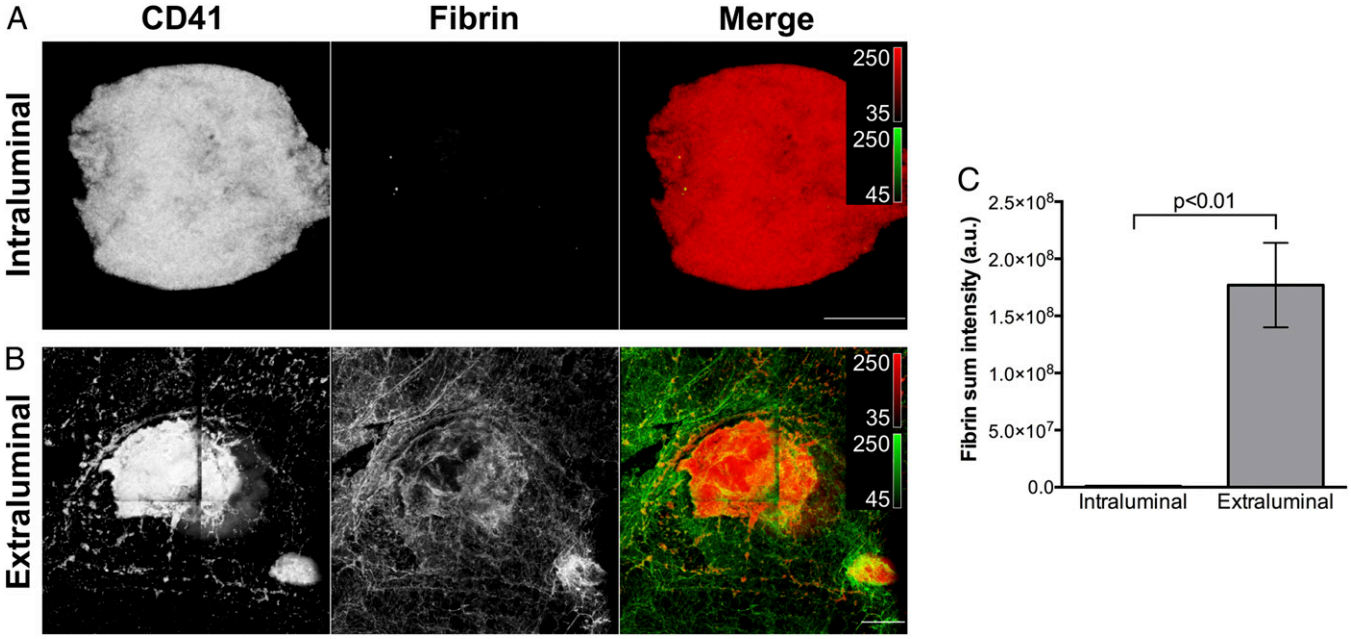

Fig. 4. Fibrin formation in the intraluminal and extravascular portions of mouse jugular vein hemostatic plugs. (*A* and *B*) Micrographs show a representative hemostatic plug fixed 5 min after puncture injury. The *Top* panels (*A*) show the intraluminal portion and *Bottom* panels (*B*) show the extraluminal portion of the same hemostatic plug imaged from each side. The images are maximum-intensity projections of a series of z-plane images acquired using 2-photon microscopy. Platelets (CD41, *Left* panels and red in the merge) and fibrin formation (*Middle* panels, green in the merge) are shown. (Scale bars: 100 μm.) (*C*) Fibrin sum fluorescence intensity in the intraluminal and extraluminal portions of hemostatic plugs. Fibrin quantification was performed on $n = 6$ hemostatic plugs as described in the *SI Appendix, Supplemental Methods*. Graphs show mean ± SEM; statistics were performed using a Student's *t* test.

columns separated by crevasses observed by SEM. By 20 min after injury, these crevasses had largely been covered over, resulting in a fairly uniform surface of minimally activated platelets (*SI Appendix*, Fig. S3*B*), although 3D reconstructions of fluorescence images demonstrated the existence of open cavities within the platelet mass. At this later point, white blood cells were observed adhering both to the intraluminal surface of the hemostatic plug as well as surrounding endothelium (*SI Appendix*, Fig. S3*B*).

Distribution of Platelet Agonists During Hemostatic Plug Formation. The dramatic differentiation of morphologic and molecular features between the intravascular and extravascular portions of hemostatic plugs suggests the biochemical microenvironments in these regions are distinct. In particular, the observation that highly activated platelets and fibrin are localized primarily on the extravascular side implies that thrombin activity is restricted to this region, consistent with observations from prior studies in smaller vessels (9, 12). As additional evidence to support this conclusion, we used annexin V binding to examine the localization of phosphatidylserine-positive membranes. We found that annexin V binding showed a similar overall distribution to P-selectin positivity, although with a more punctate appearance (*SI Appendix*, Fig. S4). It was observed primarily in the extravascular space in regions of highly activated platelets.

Altered Hemostatic Plug Architecture in the Setting of $P2Y_{12}$ Antagonism Causes Bleeding. Antiplatelet therapy using a $P2Y_{12}$ antagonist is currently the standard of care in multiple patient populations with elevated risk for atherothrombosis. A common adverse event associated with antiplatelet therapy is bleeding, resulting in an increased risk for morbidity and mortality in some patient populations (13). Here, we asked how $P2Y_{12}$ antagonism compromises the architecture of large hemostatic plugs and how this leads to bleeding. Administration of a direct-acting $P2Y_{12}$ antagonist (cangrelor) immediately before jugular vein injury resulted in a prolongation of the bleeding time in this hemostasis model. The intravascular portion of hemostatic plugs formed in the presence of cangrelor was significantly smaller than controls (Fig. 5*F*). They were largely flattened with respect to the endothelial cell surface compared with control hemostatic plugs that extended by more than 100 μm into the vessel lumen (compare Fig. 5*A* vs. Fig. 1*A*). All platelets on the intravascular side appeared minimally activated at the morphologic level, although P-selectin expression was still observed at the boundary of the injury site (Fig. 5 *C*–*E*). A residual hole with minimally activated platelets accumulated around the edges of the injury site was found in cases where bleeding did not stop within the 5-min observation period (see following).

The extravascular portion of hemostatic plugs from cangrelor-treated mice was highly variable, and in contrast to controls, it had an abundance of minimally activated platelets in addition to highly activated platelets (Fig. 6). A gradient of platelet activation was observed in which platelets farthest from the injury site were most activated, similar to the appearance of platelets on the extravascular side of control hemostatic plugs (Fig. 6*B* vs. Fig. 6*E*). Platelets closer to the injury were minimally activated, especially in cases in which the hole did not close and bleeding persisted, in contrast to the highly activated platelets found within the injury site of controls (Fig. 6*C* vs. Fig. 6*F*). Fibrin formation followed a similar spatial distribution pattern. At the periphery of the extravascular hemostatic plug, fibrin appeared similar in vehicle- and cangrelor-treated mice (Fig. 6*B* vs. Fig. 6*E*). However, fibrin was much less abundant close to the injury site in cangrelor-treated mice compared with vehicle-treated controls (Fig. 6*C* vs. Fig. 6*F*). These findings suggest that thrombin activity close to the injury site is impaired because of the convective forces of blood flowing out through the injury site.

These results regarding hemostatic plug architecture in the setting of cangrelor treatment provide an in vivo demonstration of the importance of $P2Y_{12}$ signaling for efficient platelet–platelet cohesion and closure of the injury site. Given its role in hole closure, we hypothesized that the contribution of $P2Y_{12}$ signaling to

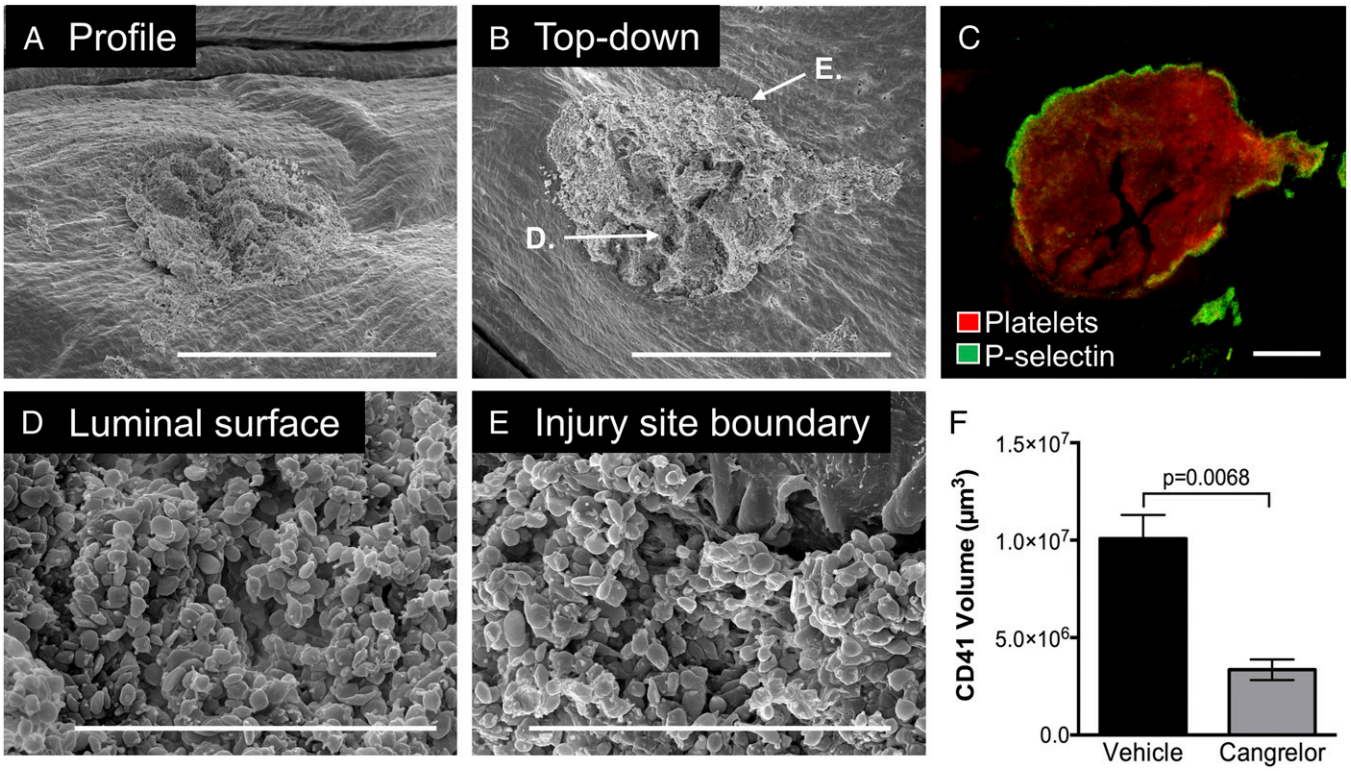

Fig. 5. The impact of $P2Y_{12}$ inhibition on intravascular hemostatic plug formation. Micrographs show a representative hemostatic plug from a cangrelor-treated mouse fixed 5 min postinjury. (*A*) Low-magnification SEM image of the intravascular portion of the hemostatic plug. (Scale bar: 300 μm.) The sample is tilted to provide a profile view. Note that the plug does not protrude into the vessel lumen substantially (compare with Fig. 1*A*). (*B*) The same hemostatic plug shown in *A* viewed from above. (Scale bar: 300 μm.) Locations of the zoomed images shown in *D* and *E* are indicated. (*C*) Fluorescence image of the same plug shown in *A* and *B*. The image is a maximum-intensity projection of a series of z-plane images acquired using 2-photon microscopy. (Scale bar: 100 μm.) (*D* and *E*) Higher-magnification SEM images of the regions of the hemostatic plug indicated in *B*. (*F*) Volume measurements of hemostatic plugs from vehicle- and cangrelor-treated mice. $n = 5$ vehicle- and 3 cangrelor-treated mice. Statistics were performed using a Student's *t* test.

the hemostatic response becomes more important as the size of the injury increases. To test this hypothesis, we created different-sized injuries in the jugular veins of vehicle- or cangrelor-treated mice. After the smallest injury, made with a 125-μm-diameter needle, the morphology of hemostatic plugs was similar to that described earlier (Fig. 7*A*). Vehicle-treated mice formed a three-dimensional platelet aggregate on the luminal side of the injury site. In cangrelor-treated mice, platelets effectively filled the hole, but the platelet aggregate did not extend substantially into the lumen of the vessel (Fig. 7 *Ai* and *Aii*). In contrast, when a much larger injury was made with a 600-μm needle, platelets failed to fill the hole in the vessel wall when cangrelor was present (Fig. 7 *Ci* and *Cii*). As a result of this disrupted architecture, hemostatic plug effectiveness was substantially impaired. There was no difference in bleeding time between vehicle- and cangrelor-treated mice with the smallest injury (Fig. 7*Aiii*). At an intermediate-sized injury of 300 μm diameter, ∼50% of the injuries did not stop bleeding within the 5-min time frame of the experiment in cangrelor-treated mice (Fig. 7*Biii*). After the largest injury (600 μm diameter), none of the cangrelor-treated mice were able to form a hemostatically effective platelet plug (Fig. 7*Ciii*). Taken together, these results demonstrate that below a threshold injury size, $P2Y_{12}$ signaling becomes dispensable for hemostasis, but as injury size increases, $P2Y_{12}$ signaling becomes critical for the formation of an effective platelet plug.

Discussion

Studies in the microcirculation have suggested a dynamic model of the hemostatic response whereby the physical microenvironment within a platelet plug regulates and is regulated by the distribution of soluble platelet agonists resulting in a gradient of platelet activation extending from the site of injury (1, 7–9, 12, 14). However, in most microcirculation experimental models, blood loss is minimal or nonexistent, questioning the extent to which this model of the hemostatic response applies to larger injuries in the macrocirculation where blood loss is a defining component. In the present study, we have addressed these questions using high-resolution correlative microscopy to examine the molecular and morphological features of hemostatic plugs formed after puncture injuries in mouse jugular veins. The results show in detail the architecture of hemostatic plugs formed in this setting, including the establishment of a gradient of platelet activation that extends across the vessel wall and into the vessel lumen, with the most activated platelets found on the extravascular side. Fibrin formation, and by extension thrombin activity, was localized primarily on the extravascular side of the vessel wall where tissue factor is found (15). Finally, we showed the consequences of $P2Y_{12}$ antagonism on hemostatic plug architecture and found that an incompetent platelet plug that does not stop blood flow through the injury site also impairs thrombin localization at the site of injury. Accordingly, the contribution of $P2Y_{12}$ signaling to formation of a competent hemostatic plug scales with the size of the hole created in the vessel wall.

The finding that hemostatic plugs formed in a large vein exhibit a gradient of platelet activation is largely consistent with previous observations in the microvasculature made by us and others. However, there are informative differences as well. Small breaches in the vessel wall of small arterioles or venules result in a characteristic hemostatic plug architecture including a region of highly active, densely packed, and degranulated platelets immediately adjacent to the injury site that is overlaid by multiple

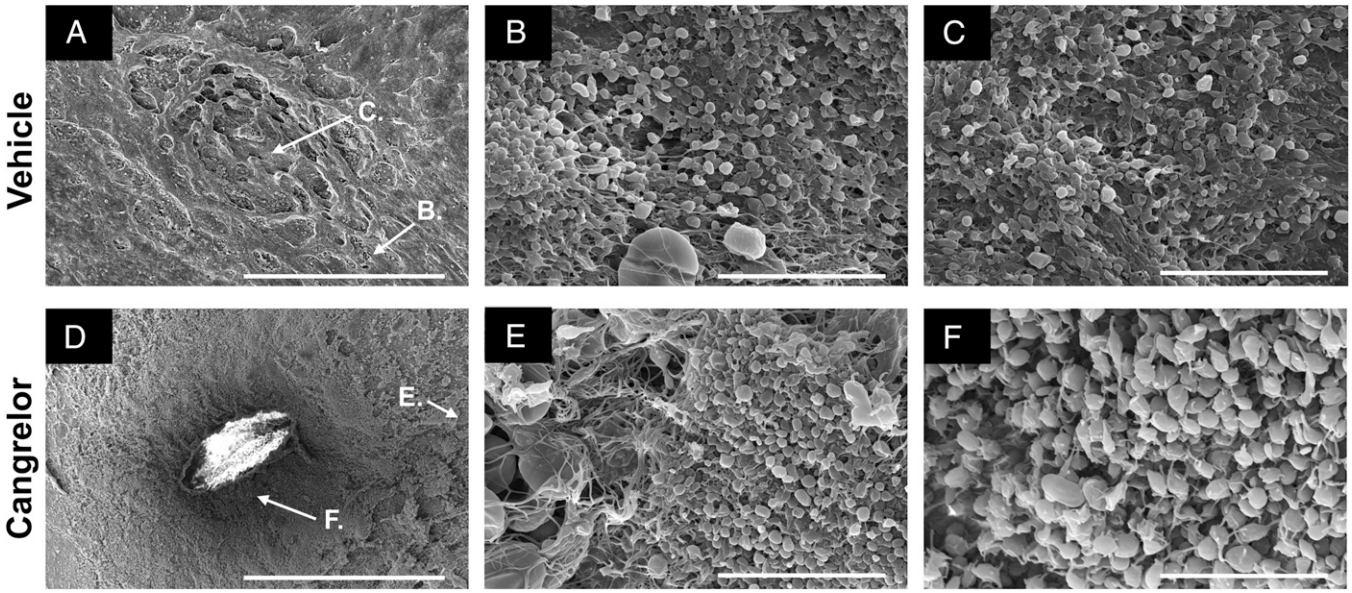

Fig. 6. The effect of $P2Y_{12}$ inhibition on extravascular hemostatic plug formation. The photomicrographs show a representative hemostatic plug from a vehicle- (*A*–*C*) or cangrelor-treated (*D*–*F*) mouse fixed 5 min postinjury. (*A* and *D*) Low-magnification SEM images of the extravascular portion of the hemostatic plug. (Scale bar: 300 μm.) Note that the hole in the vessel wall did not completely seal within the 5-min observation period in the cangrelor-treated mouse (the bright region in the center of the image in *D* is the open hole). (*B* and *E*) Higher-magnification SEM image of a region at the periphery of the hemostatic plug, as indicated by the arrows in *A* and *D*. (Scale bar: 10 μm.) Note the presence of highly activated platelets (white arrows) and regions of fibrin and red blood cells (arrowheads) in both vehicle- and cangrelor-treated mice. (*C* and *F*) Higher-magnification SEM images of a region of the hemostatic plug close to the injury site, as indicated by the arrows in *A* and *D*. (Scale bar: 10 μm.) Note that platelets in this region appear highly activated in the vehicle-treated (*C*) and minimally activated in the cangrelor-treated mouse (*F*).

layers of loosely adherent platelets that are not sufficiently activated to secrete their α-granules (12, 14). In the microcirculation studies, we referred to these populations of differentially activated platelets as the hemostatic plug "core" and "shell" regions. In the current studies in the macrocirculation, we also see regions of differential platelet activation and morphology, albeit on a much larger scale (Fig. 8). In this case, a region of highly activated, P-selectin-positive platelets is localized within the hole created by the puncture injury and extends to the extravascular space, forming a large extravascular component of the hemostatic plug. In contrast, platelets on the intravascular side of the hemostatic plug form a large 3D aggregate in which the majority of platelets are P-selectin-negative and the luminal surface shows platelets with morphologic features consistent with minimal activation. Thus, the extravascular and intravascular regions are reminiscent of the "core" and "shell" regions described in the microvasculature. These findings are consistent with prior reports dating back to the 1960s showing hemostatic plugs in multiple contexts as being composed of platelets with varying degrees of granule secretion, using transmission electron microscopy (16–19).

As in the microcirculation, the formation of a platelet activation gradient after vascular injury in a large vein is likely a result of the formation of biochemical gradients of platelet agonists. In the microcirculation, thrombin is primarily responsible for robust platelet activation leading to α-granule secretion. The colocalization of extensive fibrin formation with P-selectin-positive platelets in the present study is consistent with thrombin generation driving robust platelet activation in large vessel hemostasis. It is also consistent with the localization of phosphatidylserine-expressing membranes in which tenase and prothrombinase coagulation factor complexes assemble, which were also observed primarily on the extravascular side of hemostatic plugs. Thrombin activity is likely further restricted to the extravascular space because of the physics of the pressure drop preventing extravascular solutes from back-propagating into the lumen and the physical hindrance of transport through the platelet mass as the platelets become densely packed (5, 7, 8, 20), as well as by biochemical anticoagulant mediators such as antithrombin.

The observed differences in platelet morphology and activation state have other implications as well. Because thrombin activity appears to be restricted primarily to the outer reaches of the vessel wall, additional platelet agonists must regulate platelet aggregate formation on the intravascular side of hemostatic plugs. In the microcirculation, TxA_2/TP and ADP/$P2Y_{12}$ signaling act in concert to promote low-level platelet activation and adhesion in the outer shell region of a hemostatic plug, where thrombin activity is predicted to rapidly decline (12, 14). $P2Y_{12}$ signaling appears to play a similar role in large vein hemostasis, as inhibition of $P2Y_{12}$ signaling abrogated the formation of a large three-dimensional platelet aggregate extending into the vascular lumen. However, an important distinction between small injuries in the microvasculature and larger injuries in the macrovasculature is that $P2Y_{12}$ signaling is also required to promote platelet–platelet cohesion within the hole created by the injury in large vessels. Lack of platelet–platelet cohesion within the hole in the presence of a $P2Y_{12}$ antagonist results in increased bleeding. In contrast, in studies in the microcirculation, the holes created by the injury were not large enough to require robust platelet–platelet cohesion to plug the hole (12, 14). These findings suggest that the importance of $P2Y_{12}$ signaling during the hemostatic response scales with the size of the vascular injury. We tested this hypothesis here and showed that the increase in bleeding associated with $P2Y_{12}$ antagonism is directly linked to the size of the injury, and that below a threshold injury size, $P2Y_{12}$ signaling becomes dispensable for hemostasis. This result helps to explain the lack of a role for platelet $P2Y_{12}$ signaling in the maintenance of vascular integrity, where small breaches in the vessel wall require platelet-mediated repair (21).

The data also show that $P2Y_{12}$ antagonists affect thrombin localization. Thrombin generation and fibrin formation appear

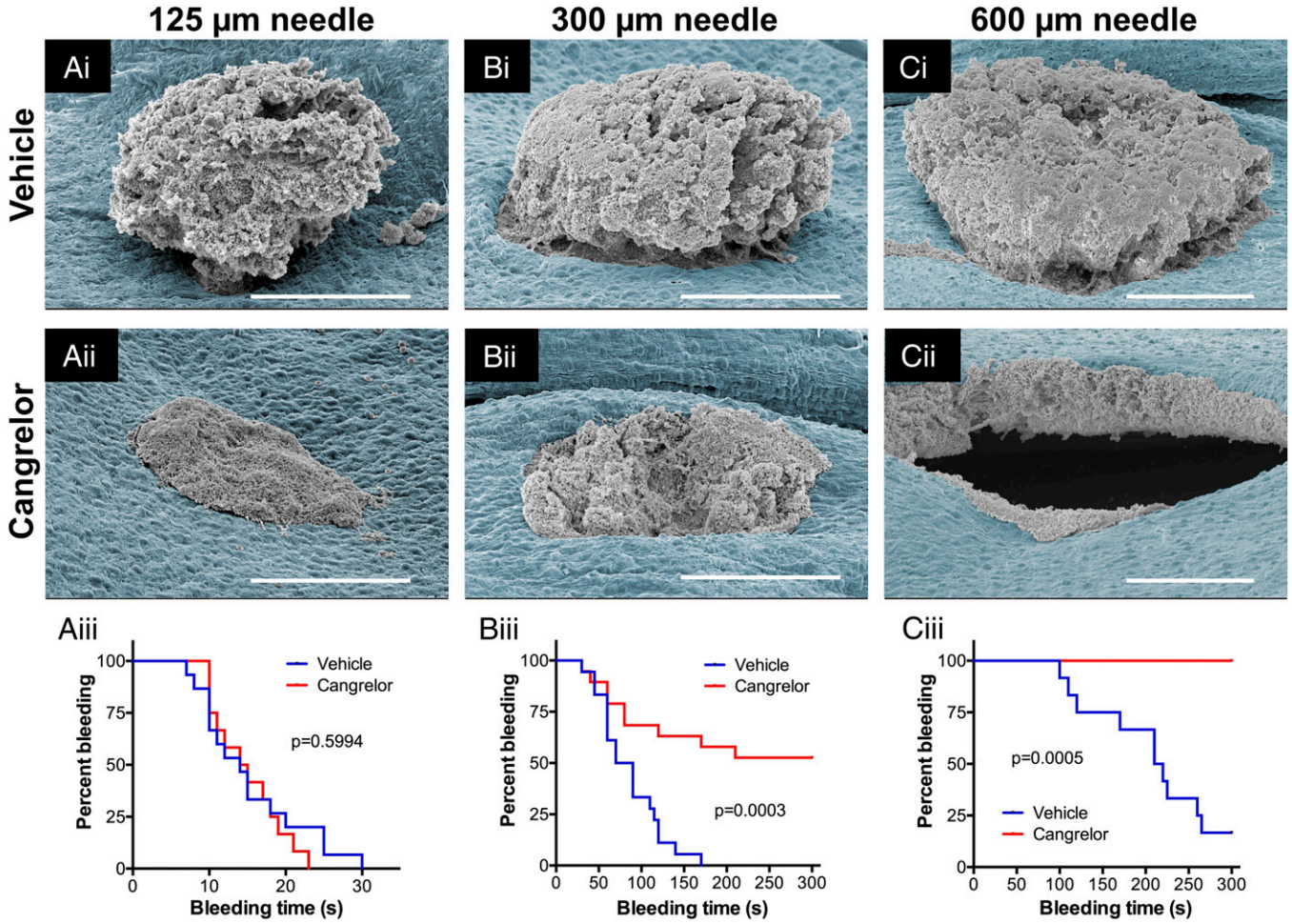

Fig. 7. The importance of $P2Y_{12}$ signaling for hemostasis increases with injury size. The photomicrographs show the intravascular portion of representative hemostatic plugs from vehicle- and cangrelor-treated mice fixed 5 min postinjury. (*A*) 125-μm-diameter needle; (*B*) 300-μm-diameter needle; and (*C*) 600-μm-diameter needle. In all cases, plugs from vehicle-treated mice are shown in the top row and cangrelor-treated mice in the second row. The intact endothelium lining the vessel is pseudocolored light blue to provide contrast. (Scale bar in all images: 100 μm.) The samples have been tilted to provide a profile view of the hemostatic plugs. Kaplan-Meier plots in the bottom row show percentage of mice bleeding versus time for vehicle- and cangrelor-treated mice subjected to puncture injuries with the indicated needle sizes (31). Experiments were terminated at 5 min postinjury (300 s). For 125 μm injury, vehicle (n = 15) and cangrelor (n = 12); 300 μm injury vehicle (n = 18) and cangrelor (n = 19); and 600 μm injury vehicle (n = 12) and cangrelor (n = 8). Statistics were performed using a log rank (Mantel-Cox) test.

normal on the extravascular side of a hemostatic plug at the periphery of the injury site, but little fibrin or robust platelet activation is seen at the injury site itself. This observation is likely explained by intact initiation of thrombin generation as a result of the tissue factor pathway, but impaired spatial propagation of thrombin generation toward the center of the hole as long as blood continues to flow through the injury site. This conclusion is consistent with computational and in vitro studies demonstrating the effect of fluid forces on the propagation of thrombin generation away from tissue factor-bearing surfaces (22, 23). Thus, in this setting, $P2Y_{12}$ antagonists exert an indirect anticoagulant activity in addition to their direct antiplatelet activity.

Just as interesting as what was observed during the hemostatic response in this study is what was not observed. One of the more obvious examples is the lack of blood cells other than platelets making up hemostatic plugs in a large vein. Erythrocyte-rich "red clots" are commonly associated with the venous circulation because of their association with deep vein thrombosis (and subsequent pulmonary embolism). Further, the formation of highly compacted red blood cell clots resulting in the formation of polyhedral-shaped erythrocytes ("polyhedrocytes") has been observed when whole blood is clotted in vitro (24) and in coronary artery thrombi harvested from patients after arterial thrombosis (myocardial infarction) (2, 3). Because of the highly compacted nature of polyhedral erythrocytes, it has been suggested that they may be an important component of the hemostatic response helping to seal a blood vessel and prevent blood loss (25). The results of the present study instead show that a compacted erythrocyte-rich clot is not required to provide a seal for damaged vessels. This role is provided by platelets. Thus, the incorporation of erythrocytes into pathologic thrombi represents a significant distinction between hemostasis and thrombosis that could potentially have value as a therapeutic target, as recently demonstrated by studies showing reduced thrombus size when erythrocyte incorporation into thrombi is attenuated (26, 27). The lack of white blood cell contribution to the hemostatic response in large veins serves as an additional distinction between hemostasis and thrombosis, as it has been reported that white blood cells are a mechanistically important component of venous thrombi (28).

Finally, the mouse jugular vein used in these studies serves as a representative vessel of the macrocirculation, and we would expect a similar hemostatic response in other large vessels with

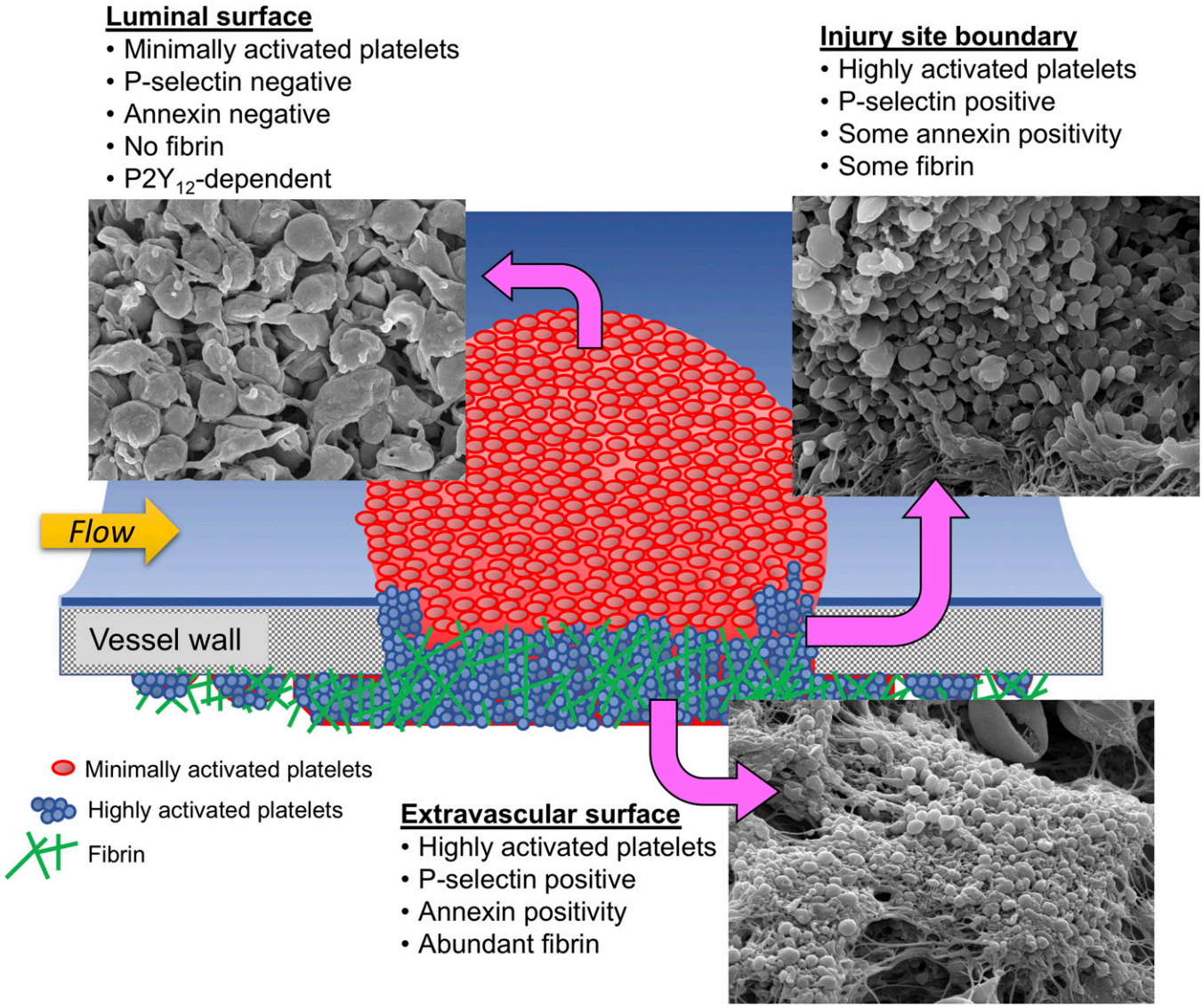

Fig. 8. Spatial heterogeneity of platelet activation and fibrin formation. An illustrated summary of the morphologic and molecular features of platelets and fibrin in different spatial domains of hemostatic plugs formed after puncture injury of mouse jugular veins. (Magnification: 5,000×.)

similar properties. However, the data also show that there are particular aspects of the hemostatic response that depend on physiologic context. Given the importance of extravasating flow and tissue factor, we anticipate that additional details of the hemostatic response, including plug architecture, the involvement of specific platelet signaling pathways, and the relative contribution of elements of the coagulation system, may vary in large vessels with different pressures, wall thickness, and tissue factor concentrations. Additional studies that explore contextual dependencies of the hemostatic response and how they relate to settings of pathologic thrombosis are clearly warranted.

In conclusion, the present study provides a characterization of the hemostatic response that takes into account the spatiotemporal regulation of coagulation and platelet activation. The results show that the distribution of platelet agonists after a breach in a larger blood vessel wall dictates as well as reflects hemostatic plug architecture, resulting in spatial heterogeneity in the extent of platelet activation and localization of fibrin formation. $P2Y_{12}$ signaling is required for efficient platelet–platelet cohesion to plug a hole in the vessel wall and allow for the spatial propagation of thrombin activity, but its contribution to hemostasis is limited to specific physiologic contexts. Taken together, these results offer insights into the organization of hemostatic plugs, provide a detailed understanding of the adverse bleeding associated with $P2Y_{12}$ antagonists, and highlight differences between hemostasis and thrombosis that may suggest alternative therapeutic approaches.

Methods

Mice and Reagents. Male C57BL/6 mice (Jackson Laboratories), 8–12 wk old, were used for all studies. The Institutional Animal Care and Use Committee of the University of Pennsylvania approved all procedures. Anti-CD41 [MWReg30, $F(ab)_2$] and anti-P-selectin (RB40.34) antibodies were purchased from BD Bioscience. Both were fluorescently labeled using Alexa Fluor (488, 568, or 647) monoclonal antibody labeling kits according to the manufacturer's instructions (Life Technologies). Fluorescently labeled fibrinogen and Annexin V were purchased from Life Technologies. All fluorescent labeling reagents were infused i.v. before performing the jugular vein injury model. Fluorescently labeled fibrinogen was used to image fibrin formation. The relatively low concentration of fibrinogen infused (25 μg/mouse) resulted in robust fluorescence only when fibrin accumulated at the injury site. This was confirmed by showing that fibrin(ogen) fluorescence overlapped entirely with an anti-fibrin antibody that does not recognize fibrinogen (29) (*SI Appendix*, Fig. S5) and was abolished in the presence of a

thrombin inhibitor (*SI Appendix*, Fig. S6). The $P2Y_{12}$ antagonist cangrelor was a generous gift from The Medicines Company. Because of its short half-life (3–6 min) (30), cangrelor was administered as an initial bolus (0.3 mg/kg), followed by a continuous infusion (0.1 mg/kg/min) via a cannula placed in the left jugular vein. Vehicle (normal saline) was administered at the same rate for control experiments.

Mouse Jugular Vein Puncture Injury. The right external jugular vein was isolated and gently cleaned of connective tissue. After infusion of fluorescently labeled imaging reagents, a puncture injury was created in the vein using either a 23-, 30-, or 35-gauge needle (600, 300, and 125 μm diameters, respectively). In all cases, the puncture injury resulted in bleeding. Extravasated blood was continually rinsed away from the injury site by slow superfusion of normal saline delivered via a syringe pump. The time to cessation of bleeding as visualized through a dissecting microscope was recorded as the bleeding time. The hemostatic response was stopped at predetermined points post-injury via transcardiac perfusion of sodium cacodylate buffer (0.2 M sodium cacodylate, 0.15 M sodium chloride at pH 7.4), followed by perfusion of 4% paraformaldehyde. After perfusion, the vein was excised, placed in a 35-mm dish coated with silicone, and submerged in paraformaldehyde. Control studies in which the vein was excised without prior perfusion wash/fixation demonstrated that this procedure did not substantially alter hemostatic plug structure. The vein was then carefully cleaned of any remaining connective tissue and either pinned to the silicone pad intact with the extravascular portion of the injury site face up or cut along its length, opened, and pinned with the intraluminal portion of the vessel face up. The vessel remained in fixative at 4 °C until fluorescence imaging was performed.

Fluorescence Microscopy. Fluorescence imaging was performed using a Leica TCS SP8 multiphoton confocal microscope with a Coherent Chameleon Vision II infrared laser, resonant scanner, and HyD nondescanned detectors. The infrared laser was used for multiphoton imaging of Alexa Fluors 488 and 568 at an excitation wavelength of 780 nm. Alexa 647 imaging was performed using traditional visible light excitation (640 nm DPSS laser). A 25× (1.0 NA) water dipping objective was used. All images were acquired using LAS X imaging software (Leica Microsystems) and analyzed using Slidebook 6.0 imaging software (Intelligent Imaging Innovations). For each hemostatic plug, a stack of z-plane images (1,024 × 1,024 pixels) with 2.5–5 μm spacing was acquired. For the extraluminal portion of hemostatic plugs that exceeded a single field of view, composite images of multiple fields of view were acquired and stitched together, using the LAS X imaging software. Isosurface view 3D reconstructions included in *SI Movies* were created using Volocity imaging software (PerkinElmer). A detailed description of fluorescence image quantification is included in the *SI Appendix*.

SEM. After fluorescence imaging, the jugular vein samples were processed for imaging by SEM, as previously described (24). Briefly, the samples were rinsed three times for 15 min with sodium cacodylate buffered solution, dehydrated serially for 15 min each in 30, 50, 70, 90, and 95 vol% ethanol, and last, three times with 100 vol% ethanol, and then rinsed twice for 15 min with hexamethyldisilazane and left to dry overnight. A thin film of gold-palladium was layered on the samples, using a sputter coater (Quorum Q 150T ES; Quorum Technologies). Micrographs were taken using a Quanta FEG250 scanning electron microscope (FEI) at 10 mm working distance. Scale bars are indicated on each micrograph.

Supplemental Materials. *SI Movies* showing z-series images and 3D reconstructions are included. *SI Appendix* files accompany Figs. 1 and 2. Additional *SI Appendix* figures as well as video and dataset legends are included in the *SI Appendix* file.

ACKNOWLEDGMENTS. We thank Andrea Stout and the Cell and Developmental Biology Microscopy Core at the University of Pennsylvania for assistance with 2-photon imaging and the Electron Microscopy Research Laboratory for assistance with SEM imaging. The authors gratefully acknowledge research funding from the National Heart, Lung, and Blood Institute (Grants P01-HL040387 and P01-HL120846 to T.J.S. and L.F.B.) and the Early Career Investigator Award from the Bayer Hemophilia Awards Program (to M.T.).

1. Stalker TJ, et al. (2014) A systems approach to hemostasis: 3. Thrombus consolidation regulates intrathrombus solute transport and local thrombin activity. *Blood* 124: 1824–1831.
2. Silvain J, et al. (2017) Thrombus composition in sudden cardiac death from acute myocardial infarction. *Resuscitation* 113:108–114.
3. Silvain J, et al. (2011) Composition of coronary thrombus in acute myocardial infarction. *J Am Coll Cardiol* 57:1359–1367.
4. Sevitt S (1974) The structure and growth of valve-pocket thrombi in femoral veins. *J Clin Pathol* 27:517–528.
5. Tomaiuolo M, et al. (2014) A systems approach to hemostasis: 2. Computational analysis of molecular transport in the thrombus microenvironment. *Blood* 124: 1816–1823.
6. Voronov RS, Stalker TJ, Brass LF, Diamond SL (2013) Simulation of intrathrombus fluid and solute transport using in vivo clot structures with single platelet resolution. *Ann Biomed Eng* 41:1297–1307.
7. Welsh JD, et al. (2016) A systems approach to hemostasis: 4. How hemostatic thrombi limit the loss of plasma-borne molecules from the microvasculature. *Blood* 127: 1598–1605.
8. Welsh JD, et al. (2014) A systems approach to hemostasis: 1. The interdependence of thrombus architecture and agonist movements in the gaps between platelets. *Blood* 124:1808–1815.
9. Welsh JD, et al. (2017) Hierarchical organization of the hemostatic response to penetrating injuries in the mouse macrovasculature. *J Thromb Haemost* 15:526–537.
10. Gross PL, Furie BC, Merrill-Skoloff G, Chou J, Furie B (2005) Leukocyte-versus microparticle-mediated tissue factor transfer during arteriolar thrombus development. *J Leukoc Biol* 78:1318–1326.
11. Getz TM, et al. (2015) Novel mouse hemostasis model for real-time determination of bleeding time and hemostatic plug composition. *J Thromb Haemost* 13:417–425.
12. Stalker TJ, et al. (2013) Hierarchical organization in the hemostatic response and its relationship to the platelet-signaling network. *Blood* 121:1875–1885.
13. Eikelboom JW, et al. (2006) Adverse impact of bleeding on prognosis in patients with acute coronary syndromes. *Circulation* 114:774–782.
14. Shen J, et al. (2017) Coordination of platelet agonist signaling during the hemostatic response in vivo. *Blood Adv* 1:2767–2775.
15. Drake TA, Morrissey JH, Edgington TS (1989) Selective cellular expression of tissue factor in human tissues. Implications for disorders of hemostasis and thrombosis. *Am J Pathol* 134:1087–1097.
16. Wester J, Sixma JJ, Geuze JJ, van der Veen J (1978) Morphology of the early hemostasis in human skin wounds: Influence of acetylsalicylic acid. *Lab Invest* 39:298–311.
17. Hovig T, Rowsell HC, Dodds WJ, Jorgensen L, Mustard JF (1967) Experimental hemostasis in normal dogs and dogs with congenital disorders of blood coagulation. *Blood* 30:636–668.
18. Jorgensen L, Rowsell HC, Hovig T, Mustard JF (1967) Resolution and organization of platelet-rich mural thrombi in carotid arteries of swine. *Am J Pathol* 51:681–719.
19. Stehbens WE, Biscoe TJ (1967) The ultrastructure of early platelet aggregation in vivo. *Am J Pathol* 50:219–243.
20. Hathcock JJ, Nemerson Y (2004) Platelet deposition inhibits tissue factor activity: In vitro clots are impermeable to factor Xa. *Blood* 104:123–127.
21. Boulaftali Y, et al. (2013) Platelet ITAM signaling is critical for vascular integrity in inflammation. *J Clin Invest* 123:908–916.
22. Kuharsky AL, Fogelson AL (2001) Surface-mediated control of blood coagulation: The role of binding site densities and platelet deposition. *Biophys J* 80:1050–1074.
23. Okorie UM, Denney WS, Chatterjee MS, Neeves KB, Diamond SL (2008) Determination of surface tissue factor thresholds that trigger coagulation at venous and arterial shear rates: Amplification of 100 fM circulating tissue factor requires flow. *Blood* 111: 3507–3513.
24. Cines DB, et al. (2014) Clot contraction: Compression of erythrocytes into tightly packed polyhedra and redistribution of platelets and fibrin. *Blood* 123:1596–1603.
25. Litvinov RI, Weisel JW (2017) Role of red blood cells in haemostasis and thrombosis. *ISBT Sci Ser* 12:176–183.
26. Aleman MM, et al. (2014) Factor XIII activity mediates red blood cell retention in venous thrombi. *J Clin Invest* 124:3590–3600.
27. Byrnes JR, Wolberg AS (2017) Red blood cells in thrombosis. *Blood* 130:1795–1799.
28. von Brühl ML, et al. (2012) Monocytes, neutrophils, and platelets cooperate to initiate and propagate venous thrombosis in mice in vivo. *J Exp Med* 209:819–835.
29. Weiler-Guettler H, et al. (1998) A targeted point mutation in thrombomodulin generates viable mice with a prethrombotic state. *J Clin Invest* 101:1983–1991.
30. Akers WS, et al. (2010) Pharmacokinetics and pharmacodynamics of a bolus and infusion of cangrelor: A direct, parenteral P2Y12 receptor antagonist. *J Clin Pharmacol* 50:27–35.
31. Bouck EG, Zunica ER, Nieman MT (2017) Optimizing the presentation of bleeding and thrombosis data: Responding to censored data using Kaplan-Meier curves. *Thromb Res* 158:154–156.